

Searching for the Cosmic Dawn with the Hyperfine Structure Transition of Hydrogen

Michael W. Eastwood

Thesis Defense

September 3, 2018

Caltech

Gregg Hallinan
Sandy Weinreb
Larry D'Addario
Stephen Bourke → Chalmers
Jake Hartman → Google
Harish Vedantham
Jonathon Kocz
Kate Clark
Marin Anderson
Ryan Monroe
Devin Cody
David Wang

Harvard/SAO

Lincoln Greenhill
Ben Barsdell → NVIDIA
Danny Price → Swinburne
Hugh Garsden
Gianni Bernardi → SKA

OVRO

David Woody
James Lamb
OVRO staff

JPL

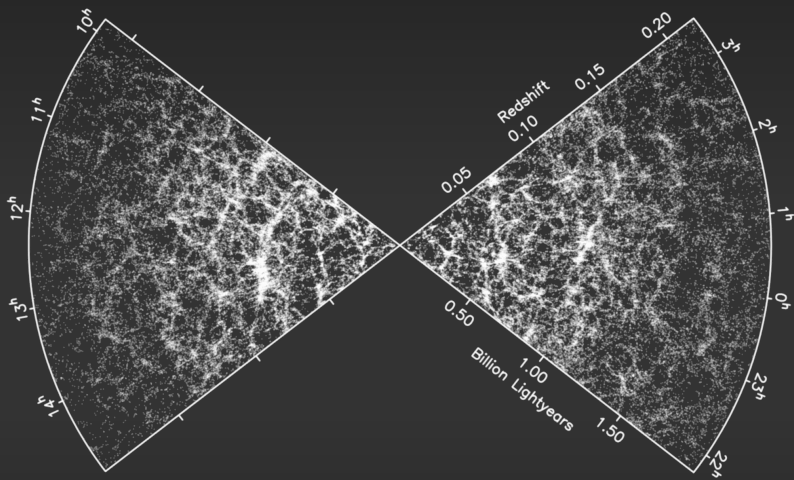
Joe Lazio

and the rest of the LWA team

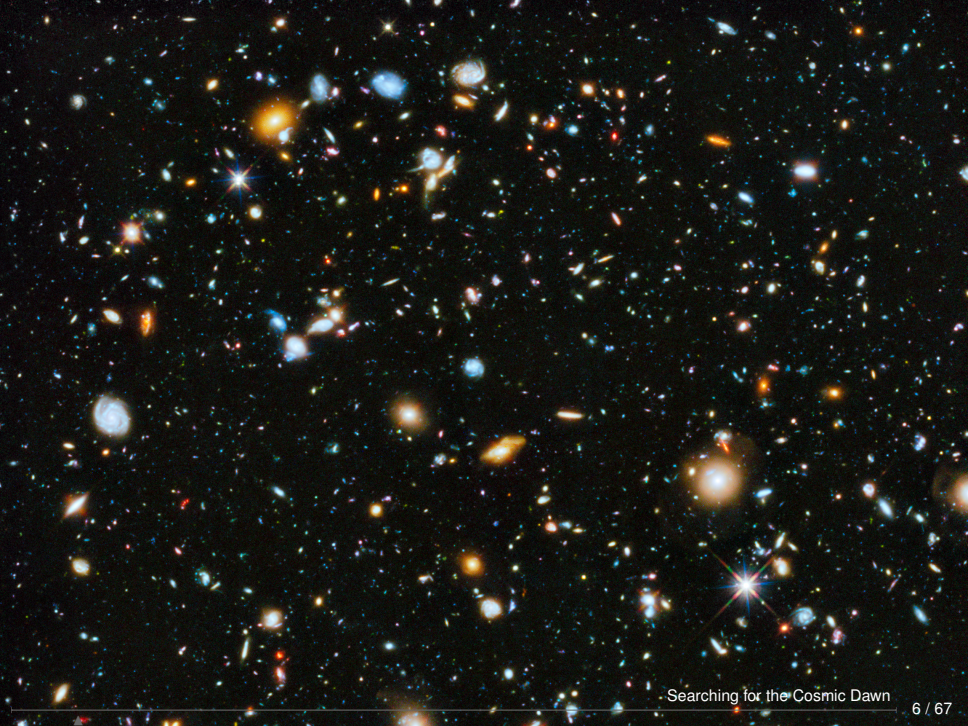
This Thesis

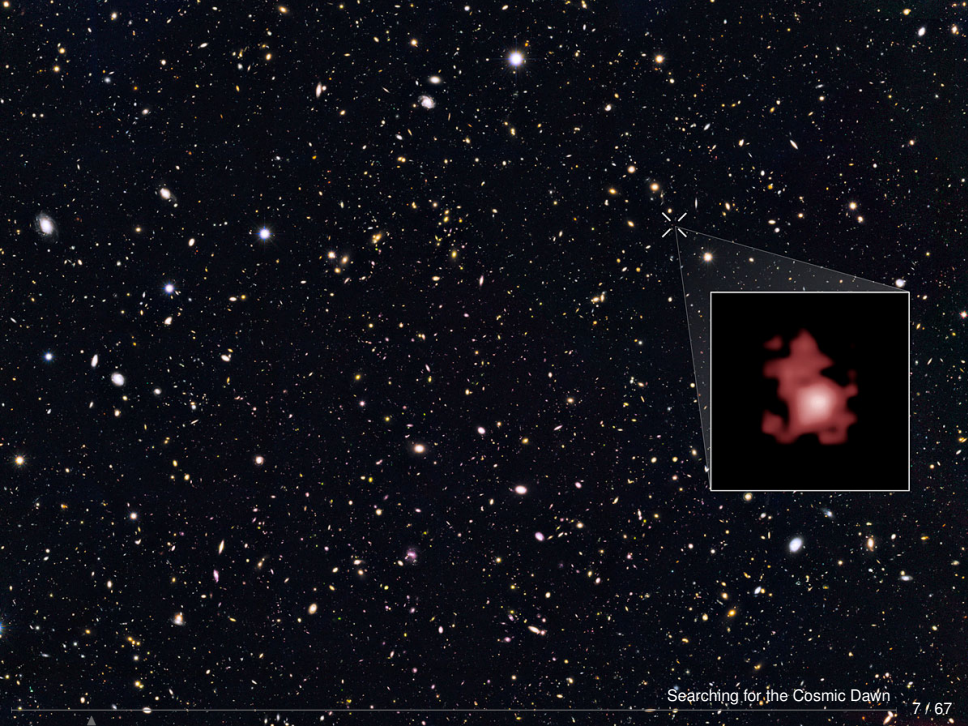
- I. Introduction to 21 cm Cosmology
- II. Commissioning the OVRO-LWA
- III. New Maps of the Sky at Meter Wavelengths
- IV. Upper Limits on the 21 cm Power Spectrum ($z > 18$)

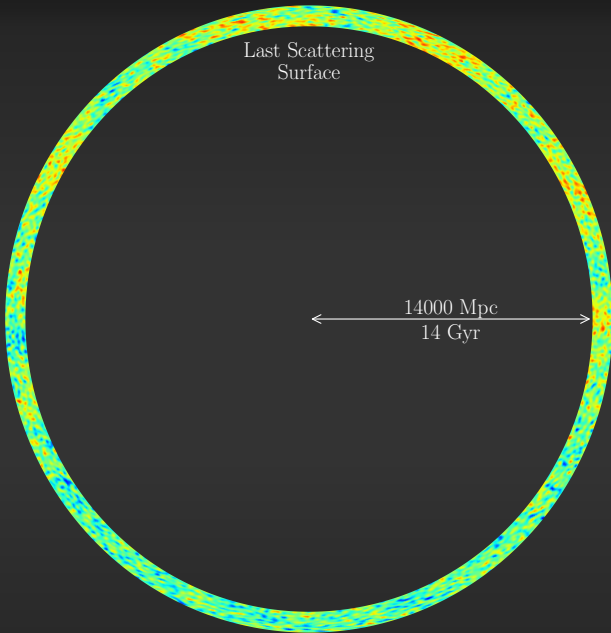
I. Introduction to 21 cm Cosmology

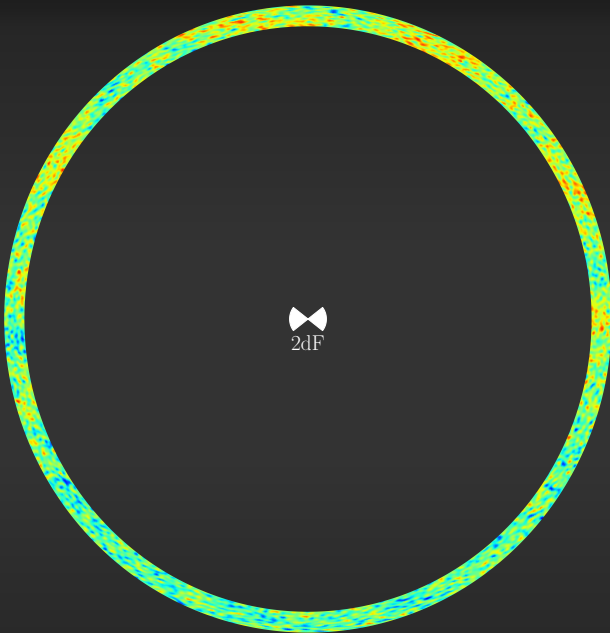


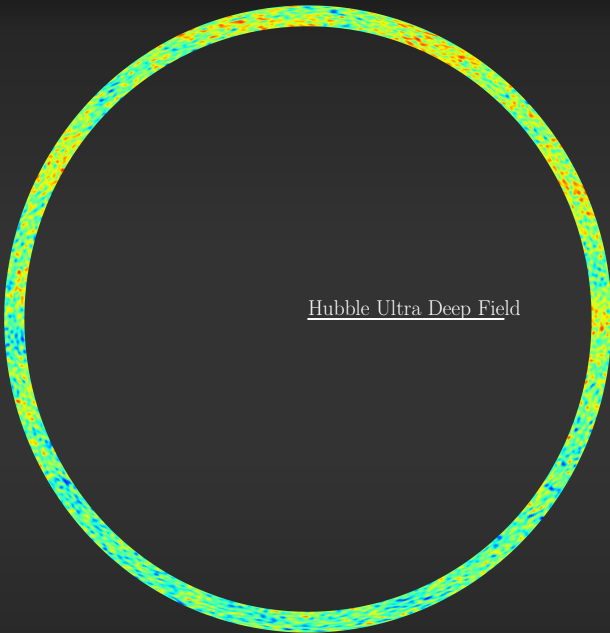
Colless et al. (2001)



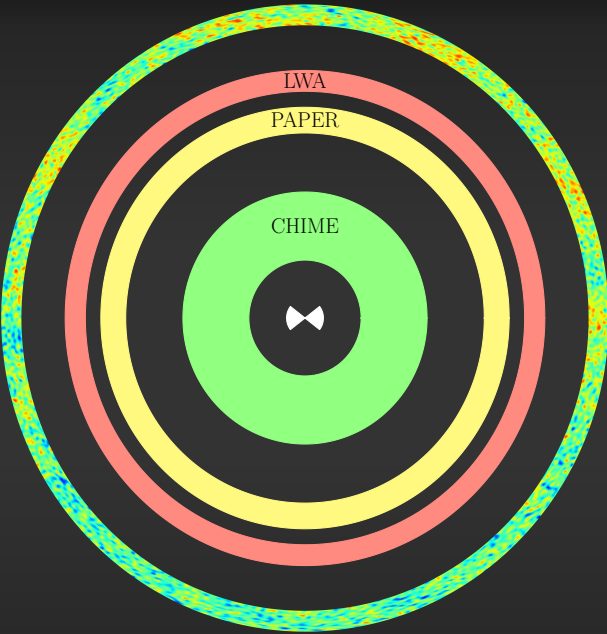


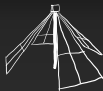




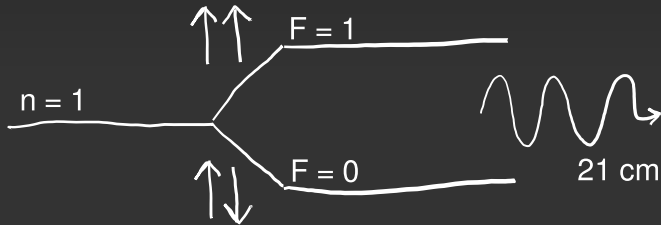


Hubble Ultra Deep Field

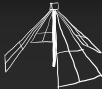




Hyperfine Structure

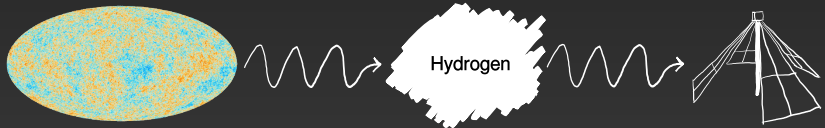


- Magnetic dipole transition → very weak
- Optically thin tracer of HI
- Spin temperature \sim excitation state



I. Introduction

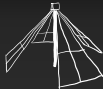
Radiative Transfer



$$T_{21} \sim 27 \left[\underbrace{x_{\text{HI}}(1 + \delta) \left(\frac{\Omega_b h}{0.0327} \right) \left(\frac{\Omega_m}{0.307} \right)^{-1/2} \left(\frac{1+z}{10} \right)^{1/2}}_{\text{quantity of HI}} \times \underbrace{\left(\frac{T_{\text{spin}} - T_{\text{CMB}}(z)}{T_{\text{spin}}} \right)}_{\text{relative temperature}} \right] \text{ mK}$$

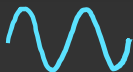
Pritchard & Loeb (2012)

Searching for the Cosmic Dawn

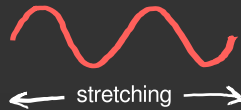


Cooling

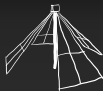
Radiation



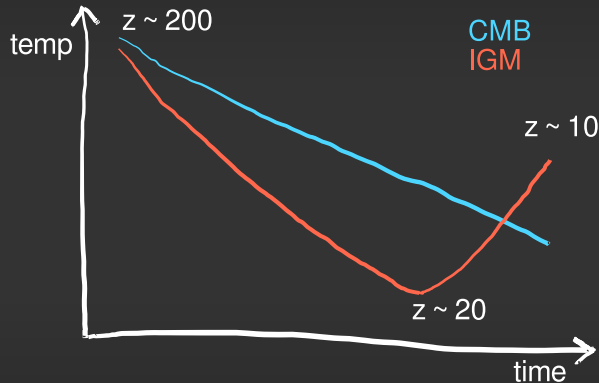
Matter

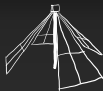


adiabatic
expansion

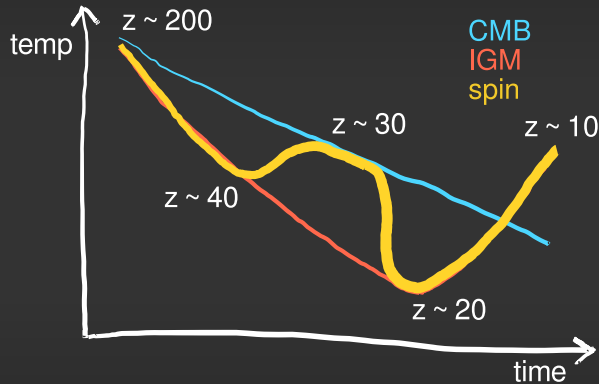


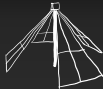
Temperature History



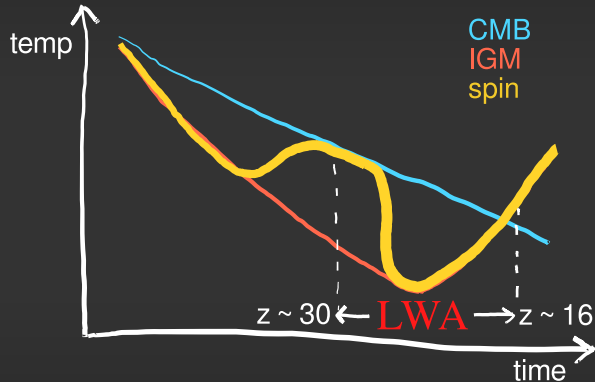


Temperature History



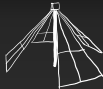


Temperature History

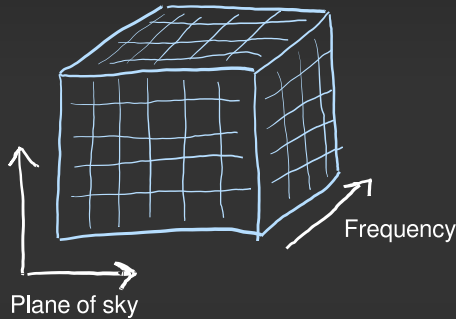




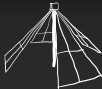
Alvarez et al. (2009)



The 3D Spatial Power Spectrum



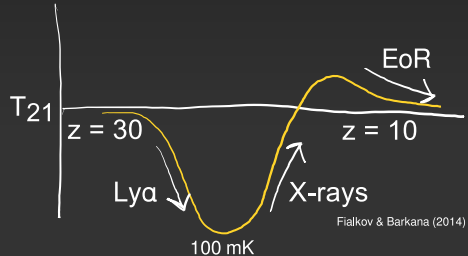
Fourier transform and square the brightness temperature in the cosmological cube.



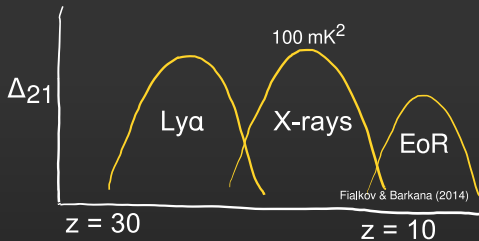
I. Introduction

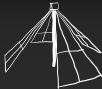
The 21 cm Signal

"COBE"
globally averaged
brightness temperature



"WMAP"
amplitude-squared of
brightness temperature
fluctuations





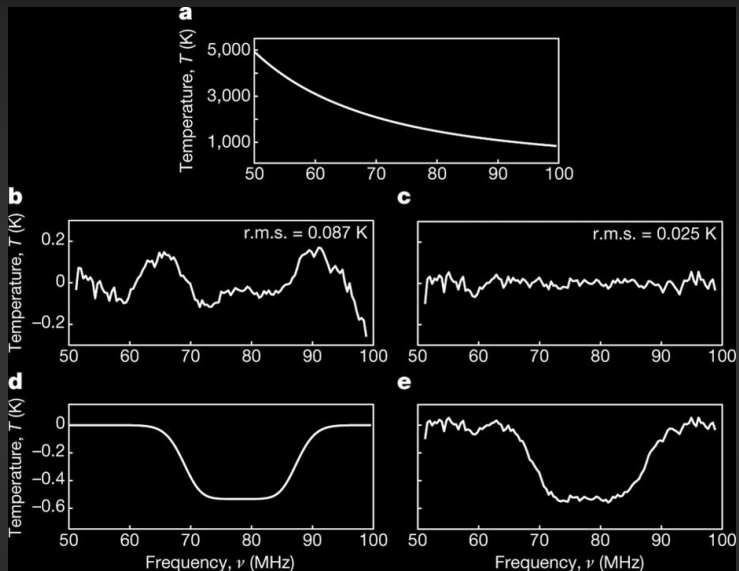
Astrophysics from the Cosmic Dawn

Effects that influence the 21 cm signal (**pre-2018**):

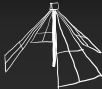
- Timing of early star formation
- Inhomogeneous star formation
- Relative motion of baryons relative to dark matter

(Tseliakhovich & Hirata 2010)

- Lyman-Werner feedback
 - (Fialkov et al. 2013)
- Flux and hardness of high-mass X-ray binaries
 - (Fialkov & Barkana 2014)



Bowman et al. (2018)



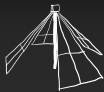
New Ideas

- Baryon–dark matter interactions
(Barkana 2018)
- New population of high-redshift radio sources
(Ewall-Wice et al. 2018)
- $\Omega_b = \Omega_m$

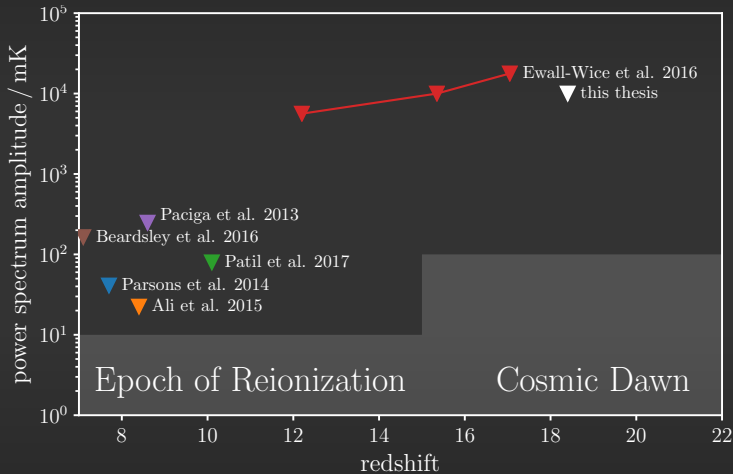
Generally, theoretical explanations of the Bowman et al. 2018 result predict an enhanced power spectrum amplitude ($\sim 7\times$).

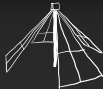
LWA GMRT LOFAR MWA PAPER





Power Spectrum Upper Limits

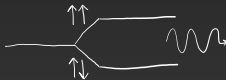




I. Introduction

Foregrounds in 21 cm Cosmology

Cosmological signal



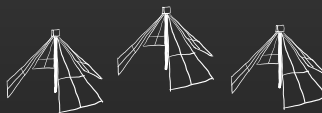
Extragalactic point sources



Galactic synchrotron emission



Ionosphere

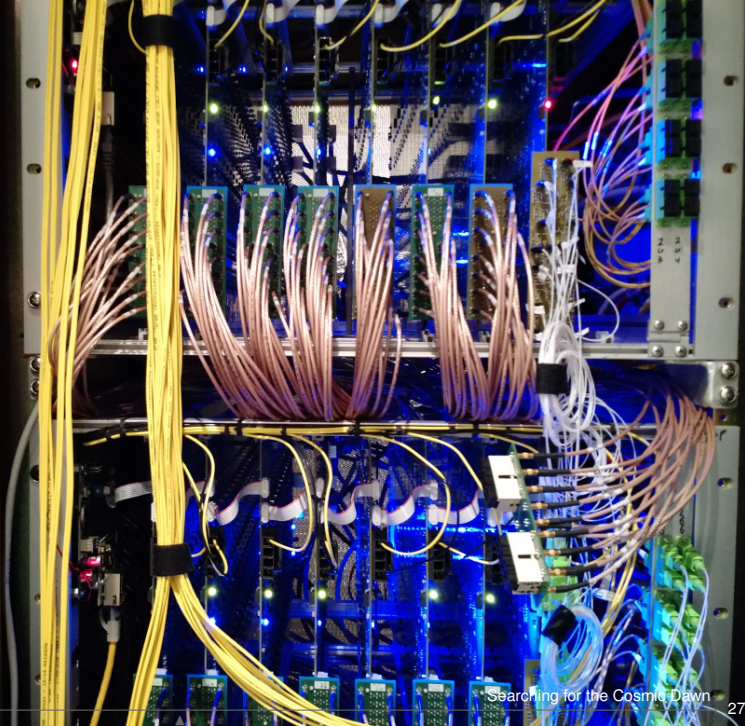


II. Commissioning the OVRO-LWA



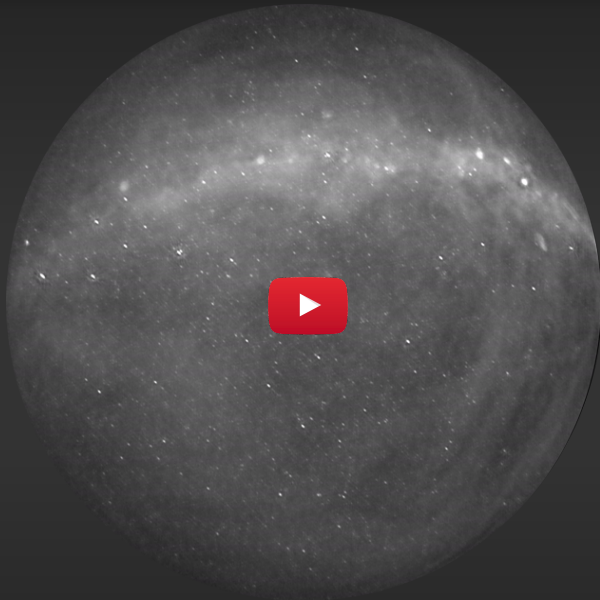












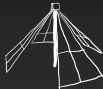


II. The OVRO-LWA

The OVRO-LWA

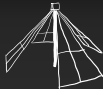
Number of Antennas	288 (256 correlated)
Core Diameter	200 m
Maximum Baseline	1.5 km
Resolution	10–20 arcmin
Frequency Range	27–85 MHz
Frequency Resolution	24 kHz
Field of View	Entire hemisphere
Integration Time (this work)	28 hr



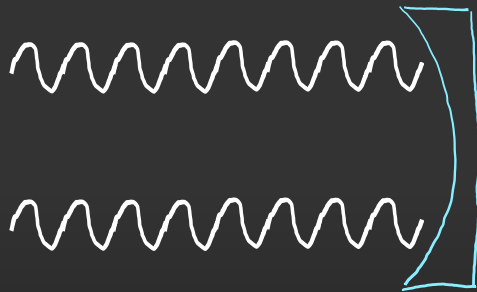


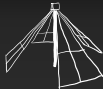
Commissioning Challenges

- Gain calibration
- Gain fluctuations
- Direction-dependent calibration
- Antenna positions
- Frequency labels
- RFI localization
- Common-mode RFI
- Primary beam mapping

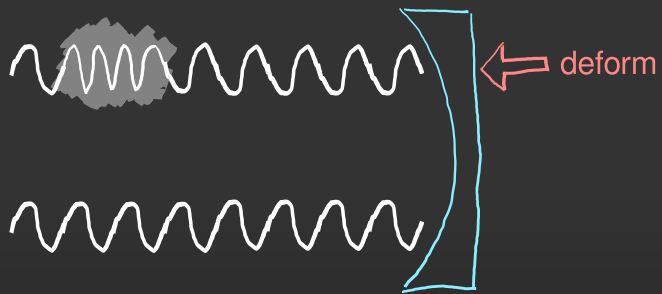


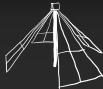
Adaptive Optics



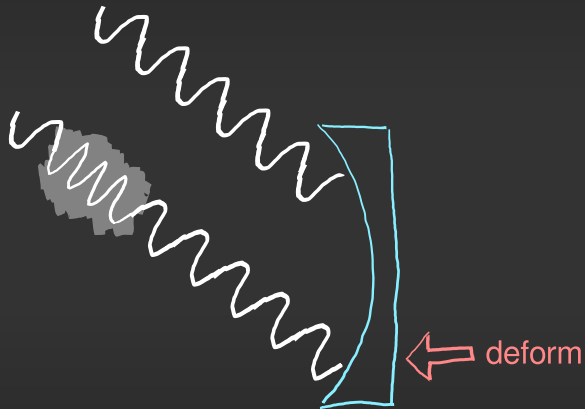


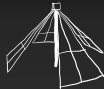
Adaptive Optics





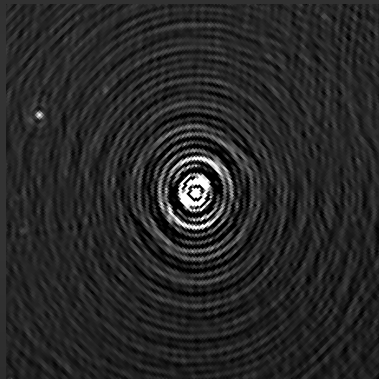
Adaptive Optics

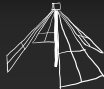




Direction-Dependent Calibration

Image of Cas A prior to removal

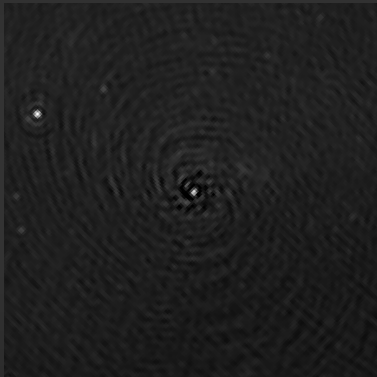


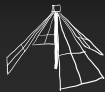


II. The OVRO-LWA

Direction-Dependent Calibration

... after removing **without** direction dependent calibration





Direction-Dependent Calibration

... after removing **with** direction dependent calibration



The Cosmic Dawn

- First generation of stars
- Formation and feedback
- Heating of the IGM
- Early X-ray sources

Transients

- Stellar flares
- Extrasolar planets
- SWIFT and LIGO follow-up
- See Anderson thesis

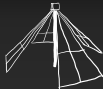
Space Weather

- Solar flares
- Jovian flares

Cosmic Rays

- Real-time detection
- See Monroe thesis

III. New Maps of the Sky at Meter Wavelengths

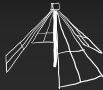


III. VHF Sky Maps

Imaging and Cleaning

$$\text{visibility} = \int (\text{sky brightness}) \times (\text{beam}) \times (\text{fringe pattern}) \, d\Omega$$

Shaw et al. (2014, 2015)



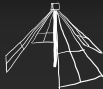
III. VHF Sky Maps

Imaging and Cleaning

$$\text{visibility} = \int (\text{sky brightness}) \times (\text{beam}) \times (\text{fringe pattern}) d\Omega$$

visibility $\xrightarrow{\text{sidereal time Fourier transform}}$ m-mode

Shaw et al. (2014, 2015)



III. VHF Sky Maps

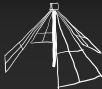
Imaging and Cleaning

$$\text{visibility} = \int (\text{sky brightness}) \times (\text{beam}) \times (\text{fringe pattern}) d\Omega$$

visibility $\xrightarrow{\text{sidereal time Fourier transform}}$ m-mode

$$\underbrace{\begin{pmatrix} \vdots \\ \text{m-modes} \\ \vdots \end{pmatrix}}_v = \underbrace{\begin{pmatrix} \ddots & & \\ & \text{transfer matrix} & \\ & & \ddots \end{pmatrix}}_B \underbrace{\begin{pmatrix} \vdots \\ a_{lm} \\ \vdots \end{pmatrix}}_a$$

Shaw et al. (2014, 2015)



III. VHF Sky Maps

Imaging and Cleaning

$$\text{visibility} = \int (\text{sky brightness}) \times (\text{beam}) \times (\text{fringe pattern}) d\Omega$$

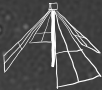
visibility $\xrightarrow{\text{sidereal time Fourier transform}}$ m-mode

$$\underbrace{\begin{pmatrix} \vdots \\ \text{m-modes} \\ \vdots \end{pmatrix}}_v = \underbrace{\begin{pmatrix} \ddots & & \\ & \text{transfer matrix} & \\ & & \ddots \end{pmatrix}}_B \underbrace{\begin{pmatrix} \vdots \\ a_{lm} \\ \vdots \end{pmatrix}}_a$$

Shaw et al. (2014, 2015)

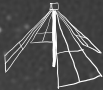
$$\hat{\mathbf{a}} = \operatorname{argmin} \left\{ \|v - B\mathbf{a}\|^2 + \varepsilon \|\mathbf{a}\|^2 \right\} = (B^* B + \varepsilon I)^{-1} B^* v$$

Eastwood et al. (2018)



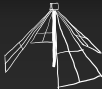
III. VHF Sky Maps

Dirty Map



III. VHF Sky Maps

Clean Map



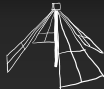
Advantages and Disadvantages

Advantages

- No gridding step
- No mosaicing step
- Exact treatment of widefield effects
- Optimal foreground filters

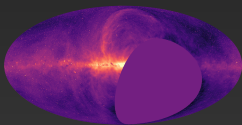
Disadvantages

- Matrix equation is block diagonal, but still large!
- 500 GB/frequency channel (!)
- Rapid ionospheric changes break assumptions

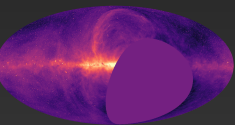


III. VHF Sky Maps

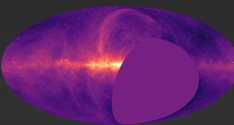
Eight New Low-Frequency Sky Maps



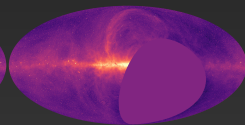
36.528 MHz



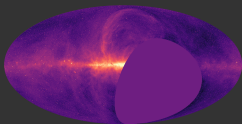
41.760 MHz



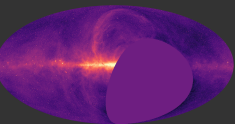
46.992 MHz



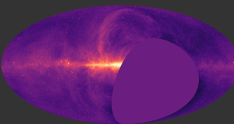
52.224 MHz



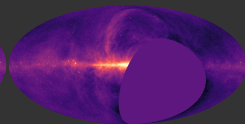
57.456 MHz



62.688 MHz



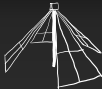
67.920 MHz



73.152 MHz

Eastwood et al. (2018)

https://lambda.gsfc.nasa.gov/product/foreground/ovrolwa_radio_maps_info.cfm

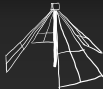


III. VHF Sky Maps

Map Properties

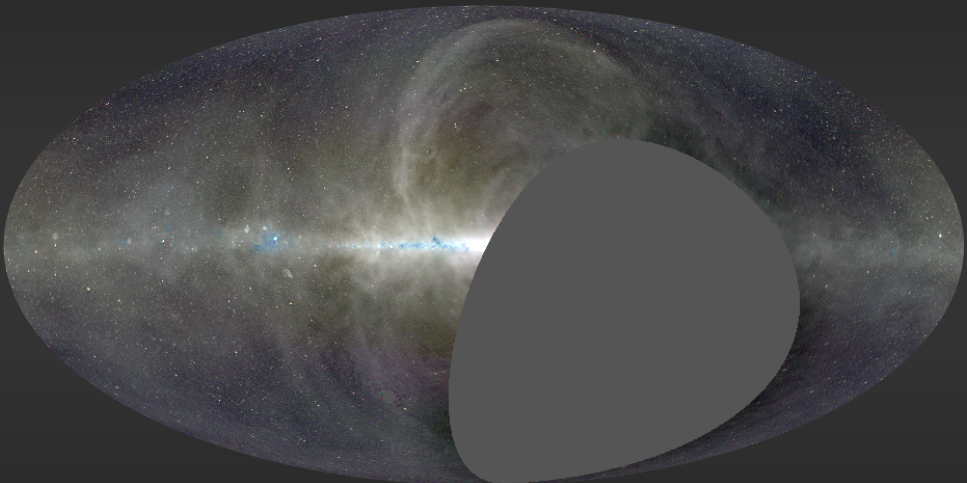
#	Frequency	Bandwidth	FWHM	Noise	
	MHz	kHz	arcmin	K	mJy/beam
1	36.528	24.	18.5	595.	799.
2	41.760	24.	17.2	541.	824.
3	46.992	24.	16.3	417.	717.
4	52.224	24.	15.6	418.	814.
5	57.456	24.	15.4	354.	819.
6	62.688	24.	15.3	309.	843.
7	67.920	24.	15.3	281.	894.
8	73.152	24.	15.7	154.	598.

Eastwood et al. (2018)

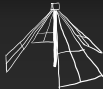


III. VHF Sky Maps

A Three Color Image

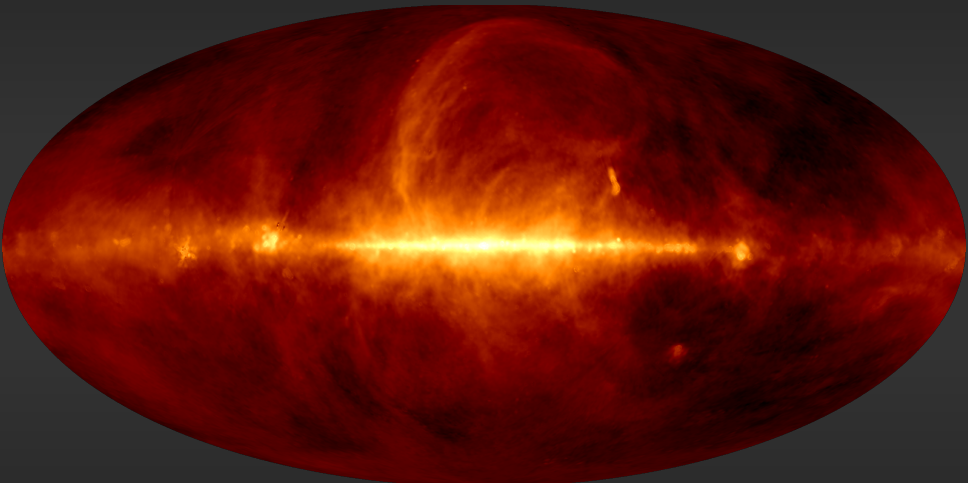


Eastwood et al. (2018)

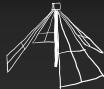


III. VHF Sky Maps

Comparison with Haslam 408 MHz

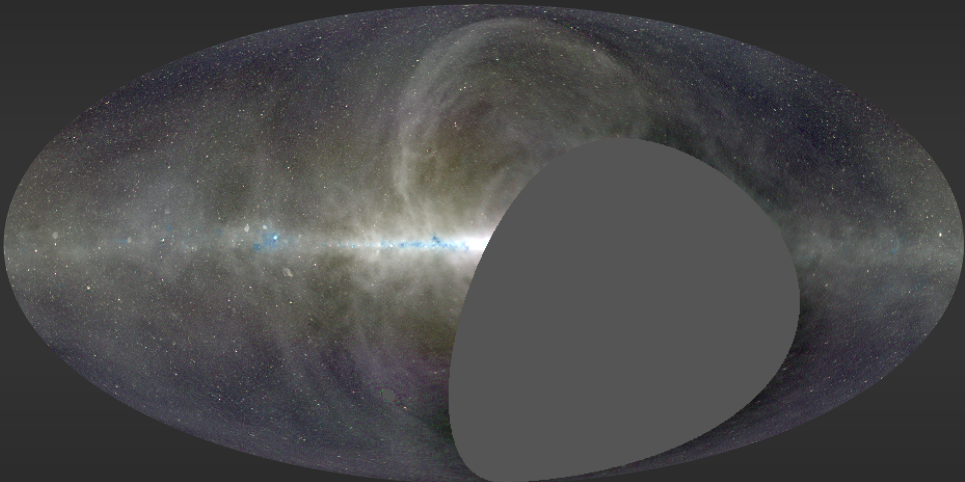


Haslam et al. (1981, 1982)

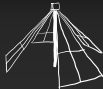


III. VHF Sky Maps

Comparison with Haslam 408 MHz

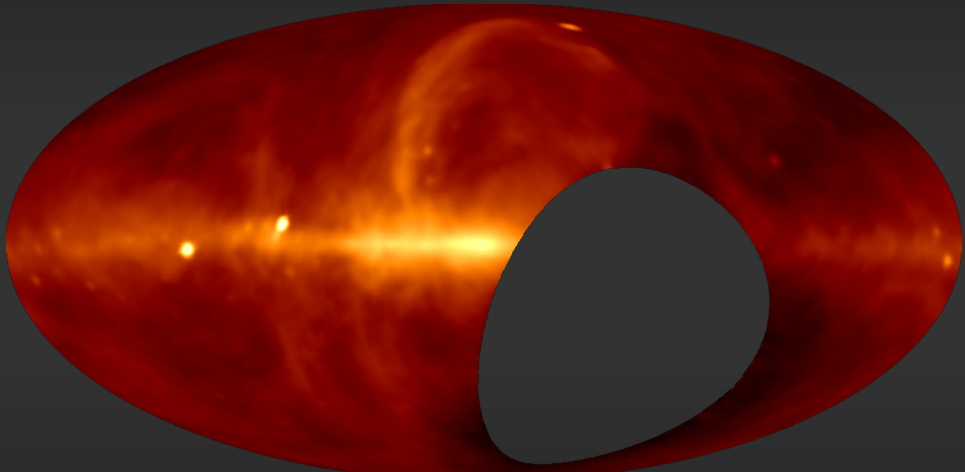


Eastwood et al. (2018)



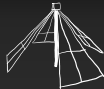
III. VHF Sky Maps

Comparison with LWA1 (35–80 MHz)



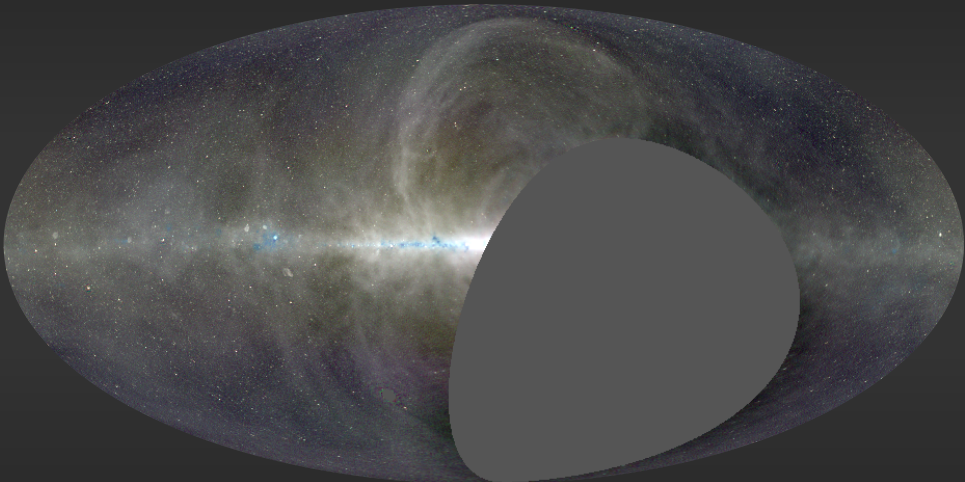
Dowell et al. (2017)

Searching for the Cosmic Dawn

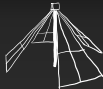


III. VHF Sky Maps

Comparison with LWA1 (35–80 MHz)

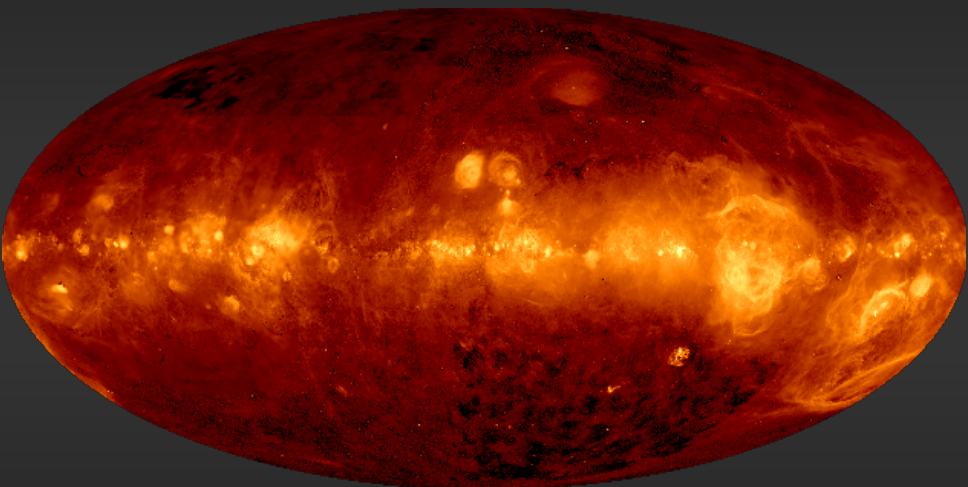


Eastwood et al. (2018)

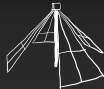


III. VHF Sky Maps

Comparison with Finkbeiner H α

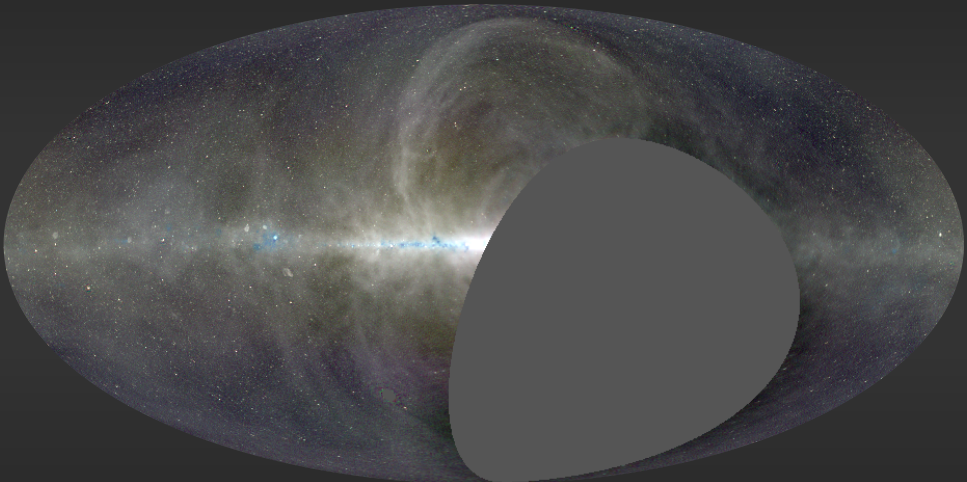


Finkbeiner et al. (2003)

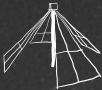


III. VHF Sky Maps

Comparison with Finkbeiner H α



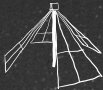
Eastwood et al. (2018)



III. VHF Sky Maps

Higher Resolution, Higher Sensitivity

Eastwood et al. (2018)



III. VHF Sky Maps

Higher Resolution, Higher Sensitivity

Eastwood et al. (in prep.)

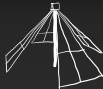


Summary

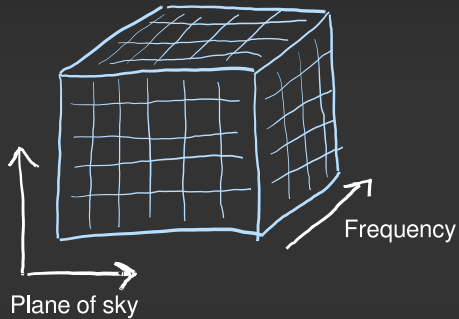
- Foreground maps are going to be extremely important for 21-cm cosmology experiments going forward.
- Creating high-fidelity foreground maps is also challenging.
- These maps are publicly available online.

https://lambda.gsfc.nasa.gov/product/foreground/ovrolwa_radio_maps_info.cfm

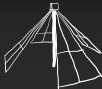
IV. Upper Limits on the 21 cm Power Spectrum ($z > 18$)



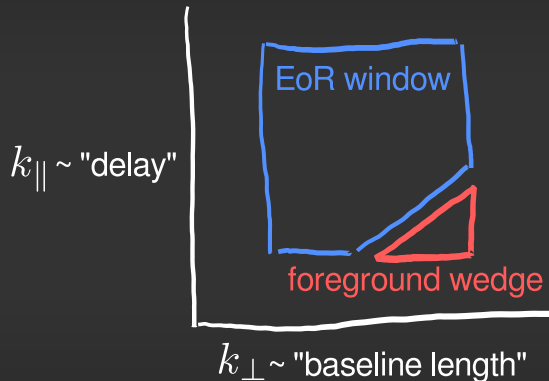
The 3D Spatial Power Spectrum

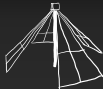


Fourier transform and square the brightness temperature in the cosmological cube.

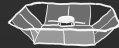
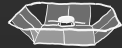
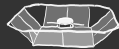
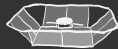
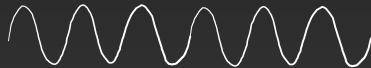


The Foreground Wedge

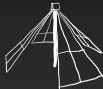




The Foreground Wedge



$k_{\perp} \sim \text{"baseline length"}$



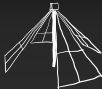
The Foreground Wedge

XF Correlator

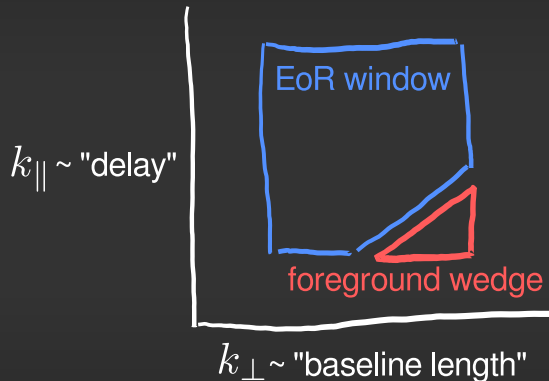
1. Cross-correlate voltages at series of time lags (“delays”)
2. Fourier transform to obtain frequency spectrum

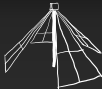
The Fourier transform along the line of sight undoes the correlator F-stage:

$$k_{\parallel} \sim \text{“delay”}$$



The Foreground Wedge

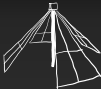




Problems with the Foreground Wedge

- **Assumes** foreground emission is “smooth enough”
- **Does not** use any information about the angular structure of the foreground emission
- **Does not** use any information about the cosmological emission
- **Does not** account for wide-field effects

Thyagarajan et al. 2015



Covariance Matrices

Key advantage of m -mode analysis: Full covariance matrices

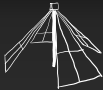
$$\langle \mathbf{v} \mathbf{v}^* \rangle = \mathbf{C} = \mathbf{C}_{21} + \mathbf{C}_{\text{fg}} + \mathbf{C}_{\text{noise}}$$

Typical size without m -mode analysis:

$$(N_{\text{baselines}} \times N_{\text{frequencies}} \times N_{\text{times}})^2 \times 128 \text{ bits} \sim 65 \text{ EB}$$

Typical size with m -mode analysis (per matrix block):

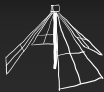
$$(l_{\max} \times N_{\text{frequencies}})^2 \times 128 \text{ bits} \sim 137 \text{ MB}$$



The Noise Covariance

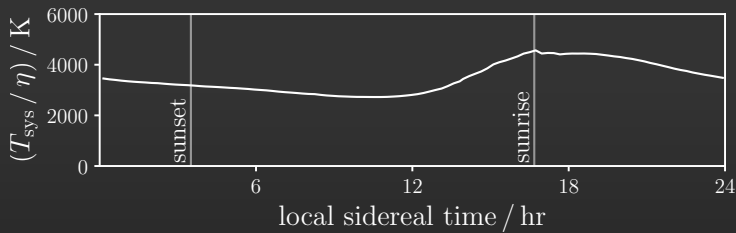
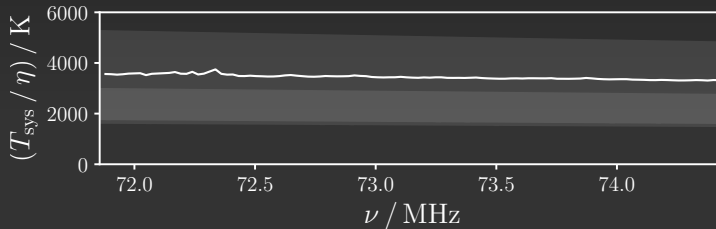
$$\langle \mathbf{v} \mathbf{v}^* \rangle = \mathbf{C} = \mathbf{C}_{21} + \mathbf{C}_{\text{fg}} + \boxed{\mathbf{C}_{\text{noise}}}$$

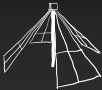
- Typically diagonal (although see Kulkarni 1989)
- Characterized by the system temperature T_{sys}
- Measured from variance of visibilities after differencing
- Expect sky noise dominated with contribution from receiver



IV. 21 cm Power Spectrum

The Noise Covariance



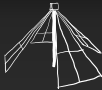


The Foreground Covariance

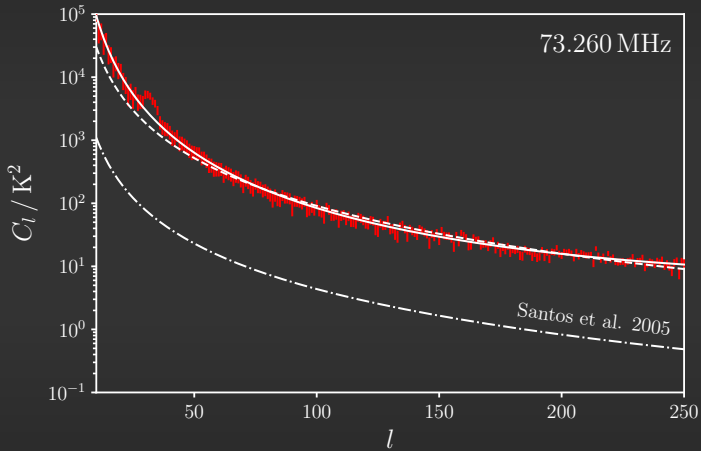
$$\langle \mathbf{v} \mathbf{v}^* \rangle = \mathbf{C} = \mathbf{C}_{21} + \boxed{\mathbf{C}_{\text{fg}}} + \mathbf{C}_{\text{noise}}$$

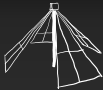
$$\left\langle a_{lm}(\nu) a_{l'm'}(\nu + \Delta\nu) \right\rangle = C_l(\nu, \Delta\nu) \delta_{ll'} \delta_{mm'}$$

- Dominated by the galactic synchrotron emission
- Contribution of point sources increases on small angular scales
- Measured $C_l(\nu, 0)$ with an optimal quadratic estimator



The Foreground Covariance





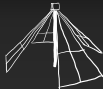
The 21 cm Signal Covariance

$$\langle \mathbf{v} \mathbf{v}^* \rangle = \mathbf{C} = [\mathbf{C}_{21}] + \mathbf{C}_{\text{fg}} + \mathbf{C}_{\text{noise}}$$

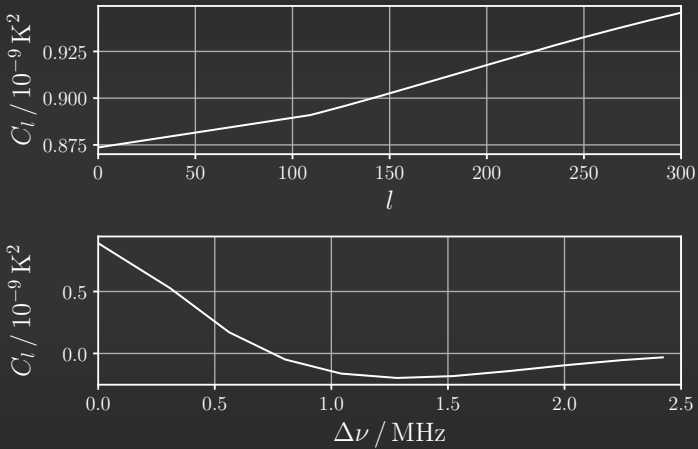
$$P_{\text{model}}(k) = \frac{2\pi^2}{k^3} \min \left[40 \left(\frac{k}{0.03 \text{ Mpc}^{-1}} \right)^2, 400 \right] \text{ mK}^2$$

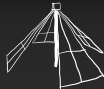
- Simple fiducial model (Fialkov et al. 2014)
- If EDGES detection is true, power spectrum amplitude reasonably expected to be 50 times brighter

(Bowman et al. 2018, Barkana 2018)



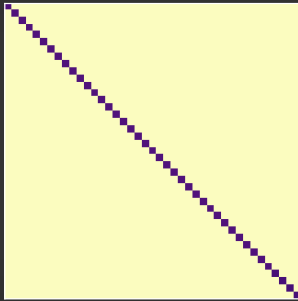
The 21 cm Signal Covariance



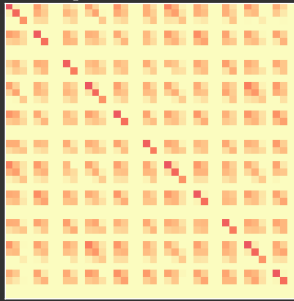


The Karhunen–Loève Transform

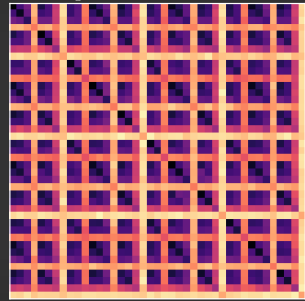
noise covariance matrix

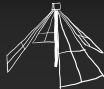


signal covariance matrix



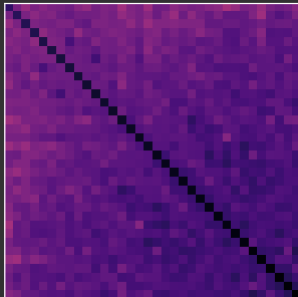
foreground covariance matrix



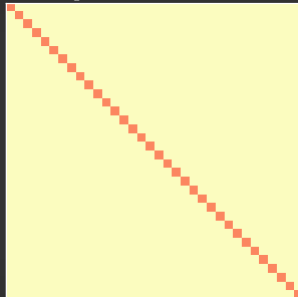


The Karhunen–Loève Transform

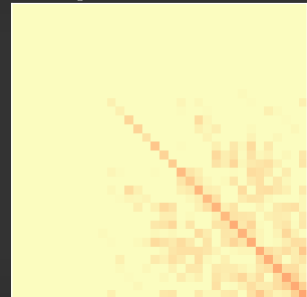
noise covariance matrix

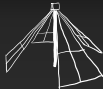


signal covariance matrix



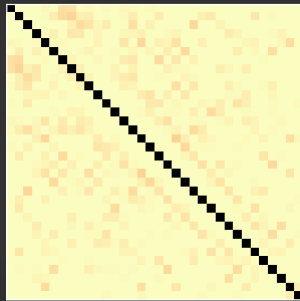
foreground covariance matrix



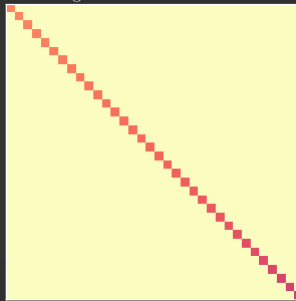


The Karhunen–Loève Transform

noise covariance matrix

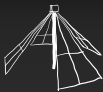


signal covariance matrix



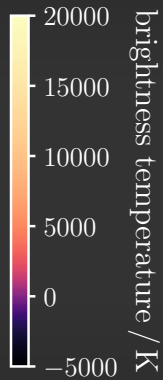
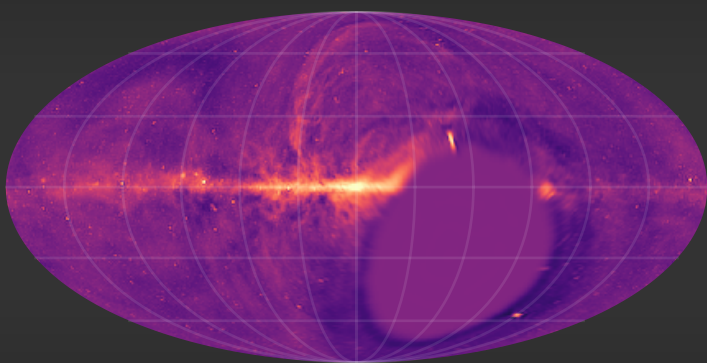
foreground covariance matrix

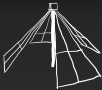




IV. 21 cm Power Spectrum

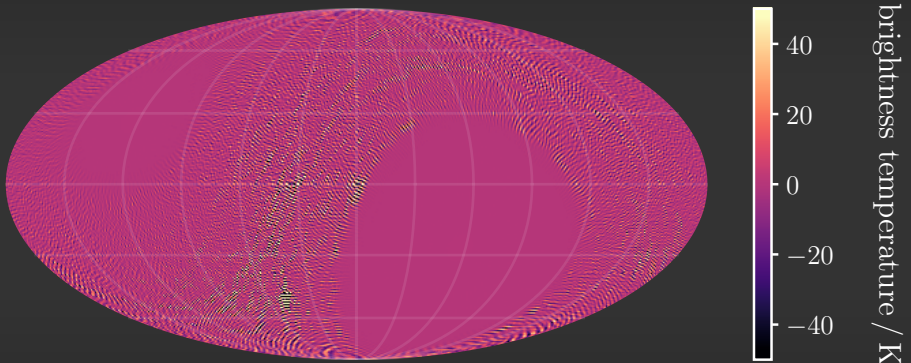
Filtered Image

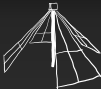




IV. 21 cm Power Spectrum

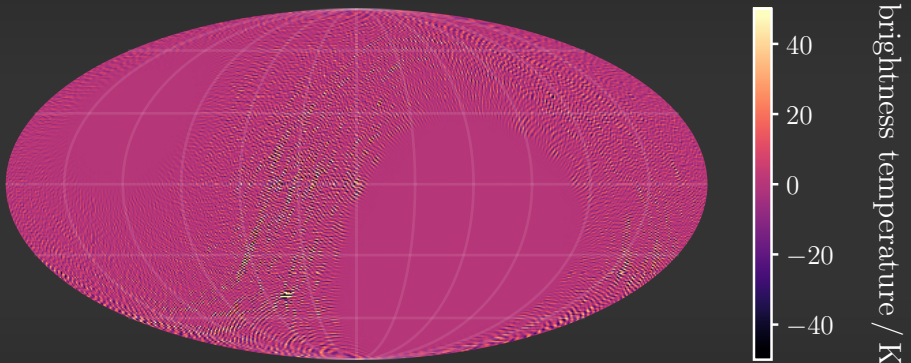
Filtered Image

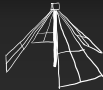




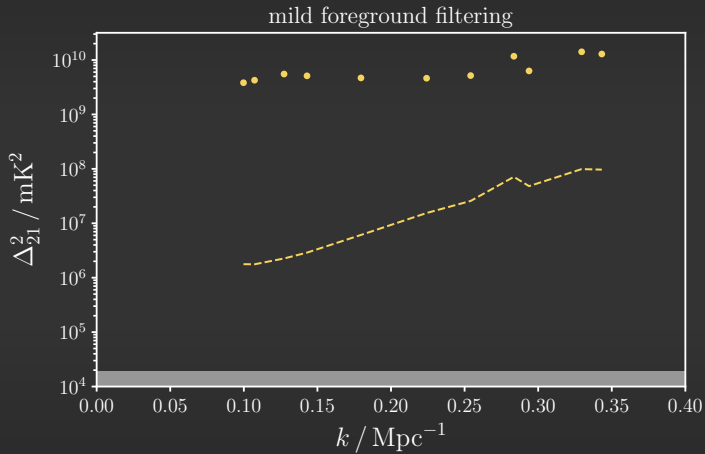
IV. 21 cm Power Spectrum

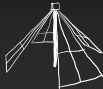
Filtered Image



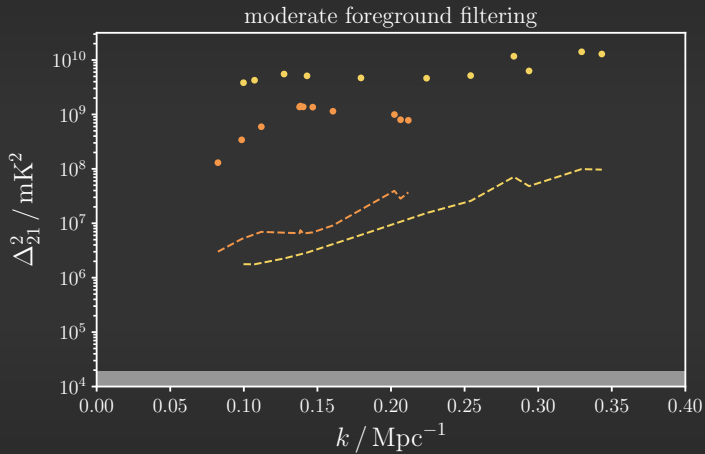


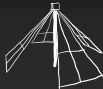
Power Spectrum Estimate



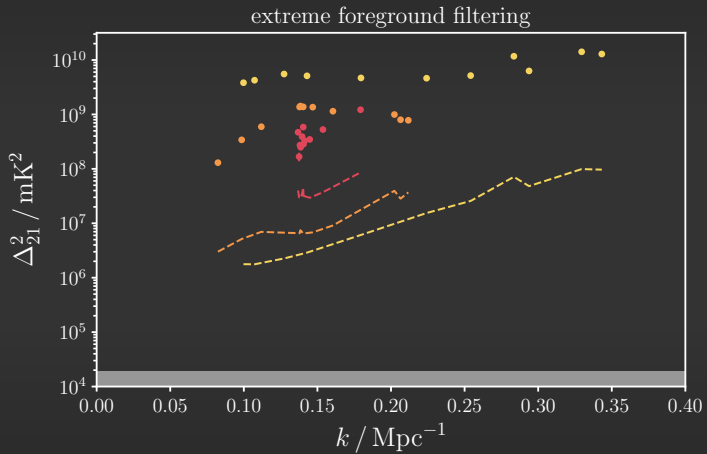


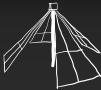
Power Spectrum Estimate





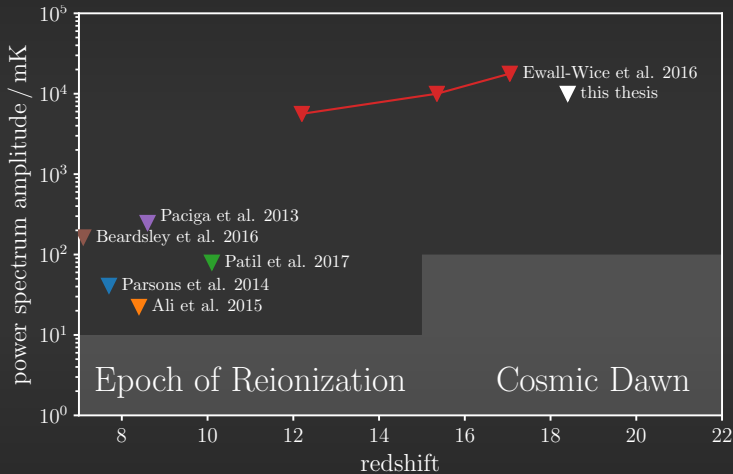
Power Spectrum Estimate

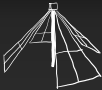




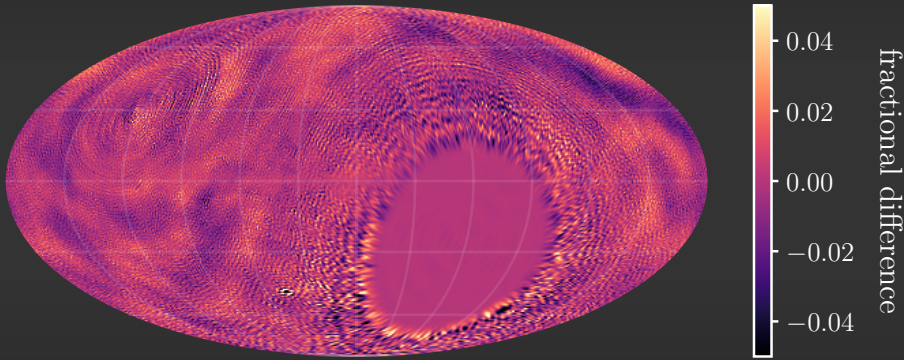
IV. 21 cm Power Spectrum

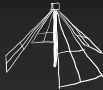
Power Spectrum Limits



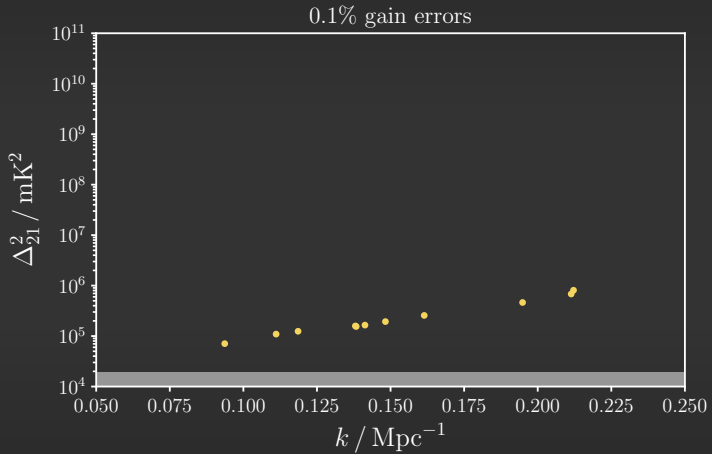


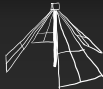
Bandpass Errors



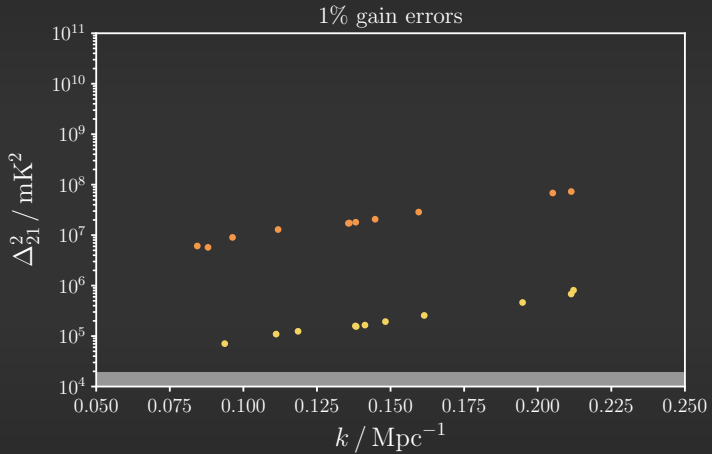


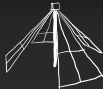
Systematic Limitations



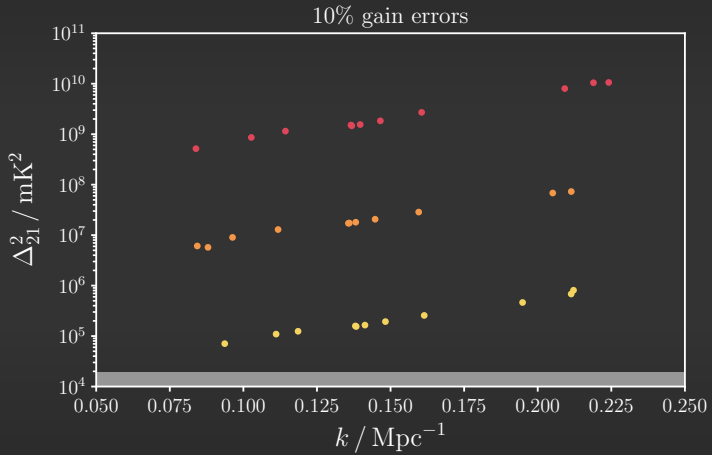


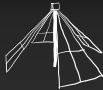
Systematic Limitations



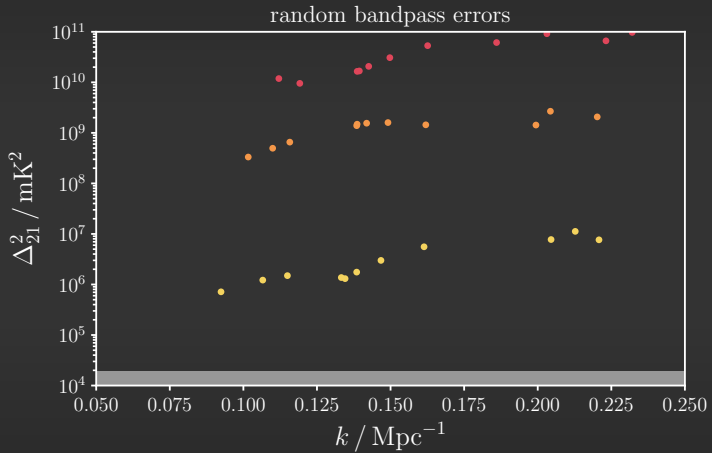


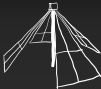
Systematic Limitations





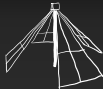
Systematic Limitations





Conclusions

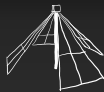
- First measured upper limit of the 21 cm power spectrum at $z > 18$
- Lowest upper limit $\Delta_{21}^2 \lesssim (10^4 \text{ mK})^2$
- The double KL transform foreground filter is effective if gain errors $< 0.1\%$ and bandpass errors $< 0.01\%$
- Current upper limits from the OVRO-LWA are consistent with $\sim 1\%$ errors in the bandpass



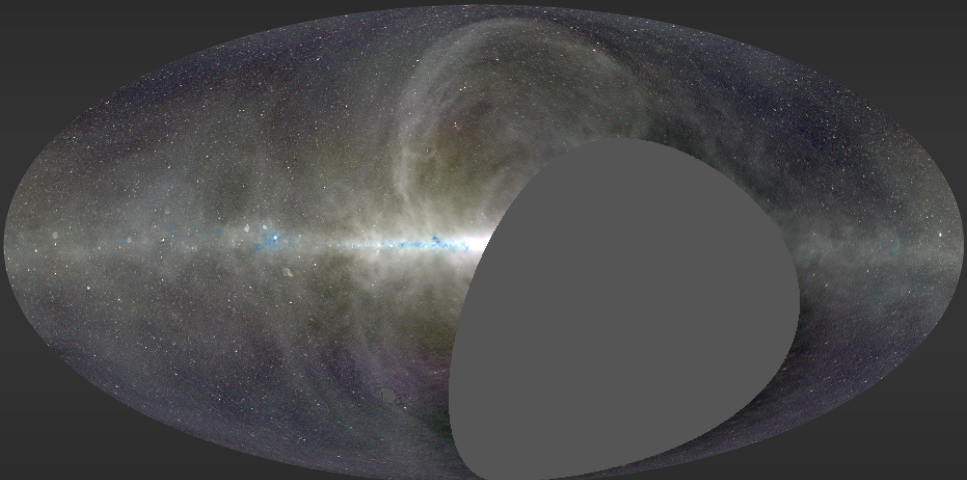
Summary

This Thesis

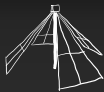
- I. Introduction to 21 cm Cosmology
- II. Commissioning the OVRO-LWA
- III. New Maps of the Sky at Meter Wavelengths
- IV. Upper Limits on the 21 cm Power Spectrum ($z > 18$)



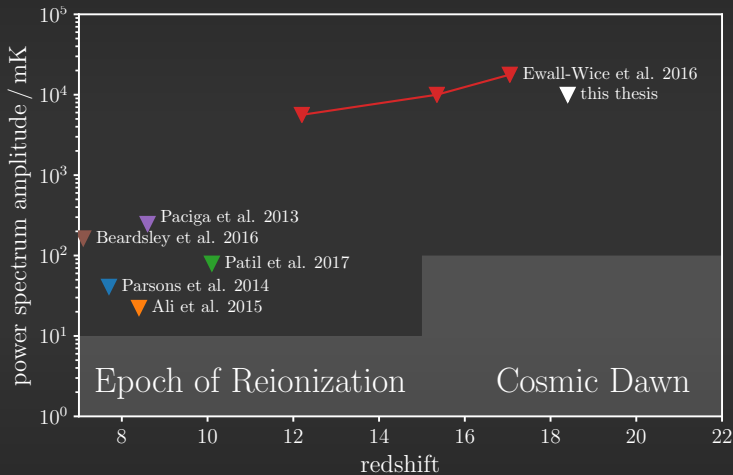
A Three Color Image



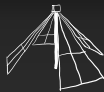
Eastwood et al. (2018)



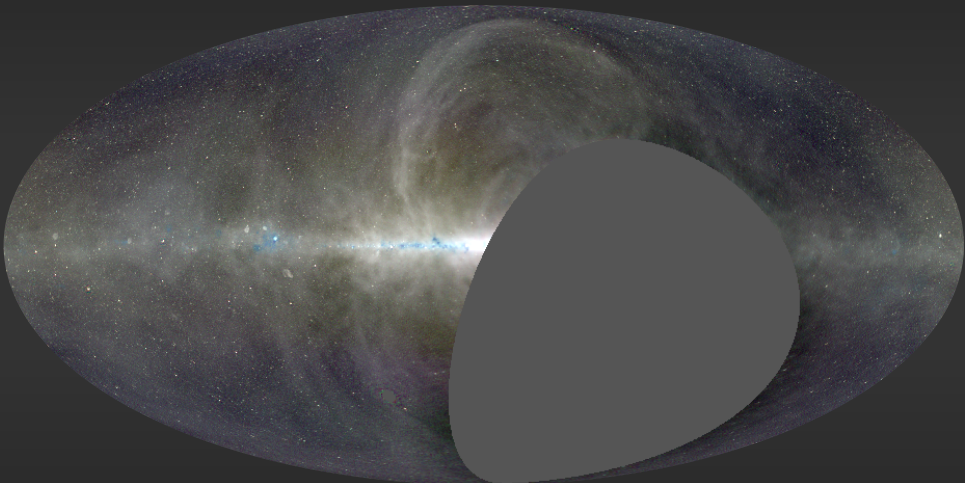
Power Spectrum Limits



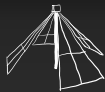
Backup Slides



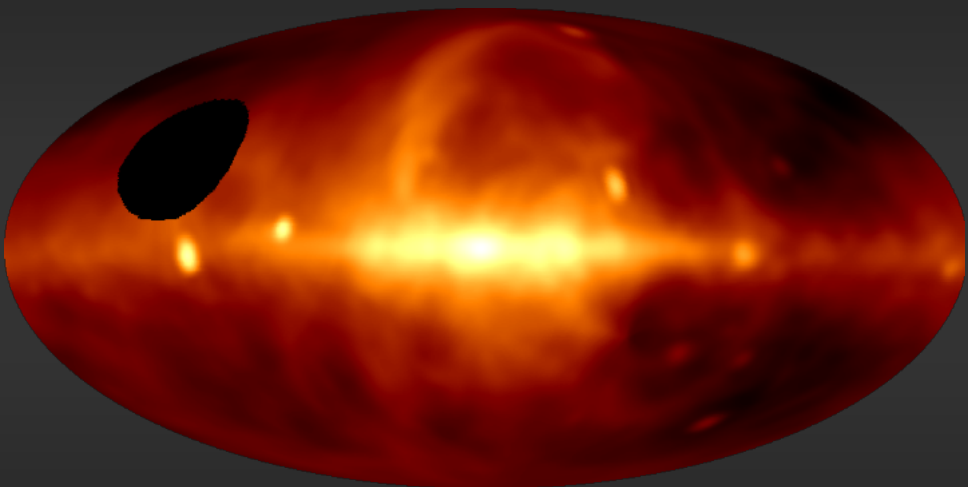
Comparison with Guzmán 45 MHz



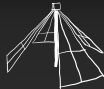
Eastwood et al. (2018)



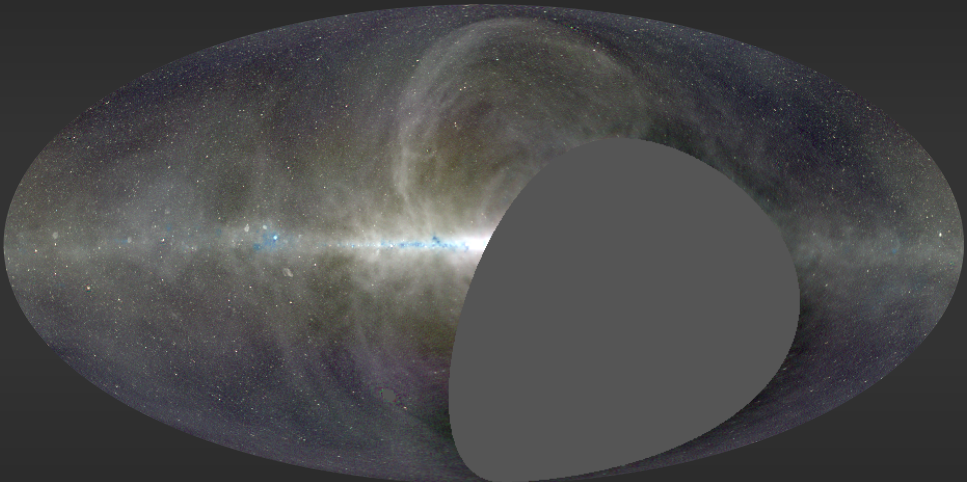
Comparison with Guzmán 45 MHz



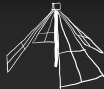
Guzmán et al. (2011)



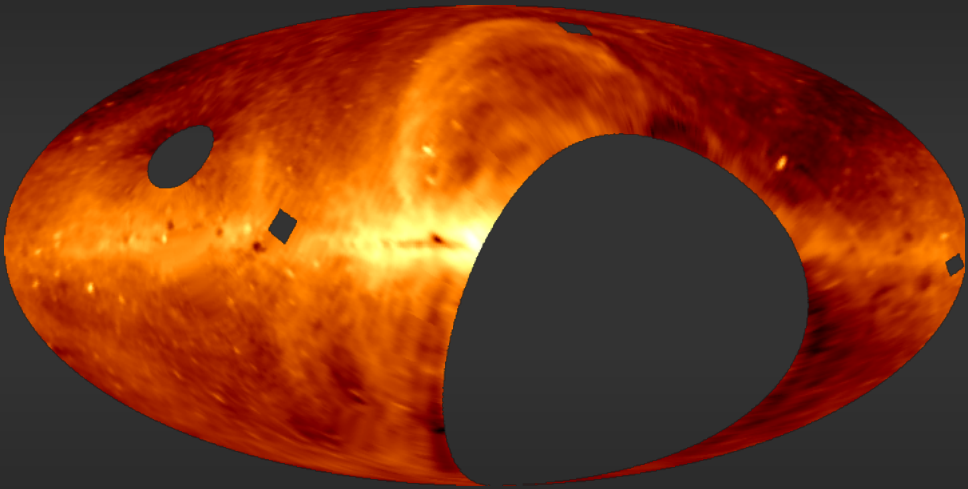
Comparison with DRAO 22 MHz



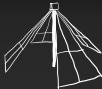
Eastwood et al. (2018)



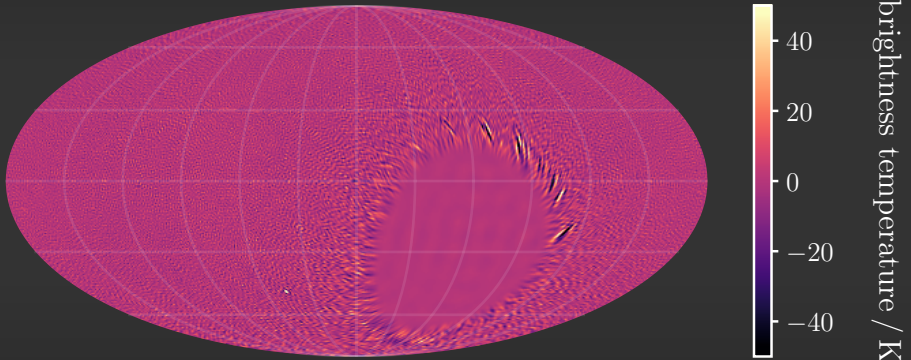
Comparison with DRAO 22 MHz

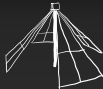


Roger et al. (1999)

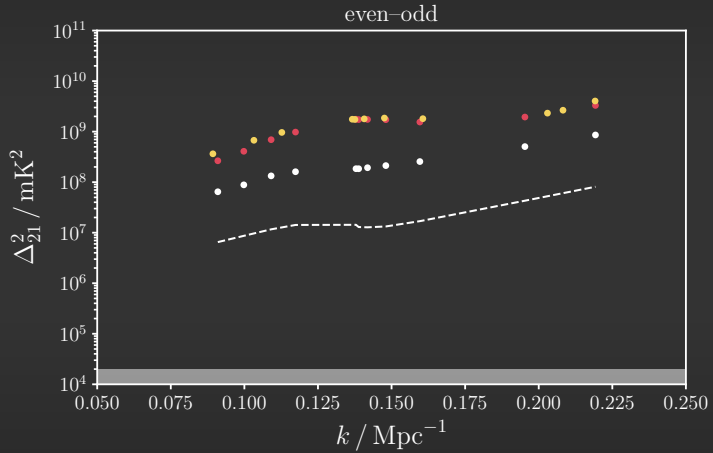


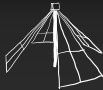
Even–Odd Jackknife



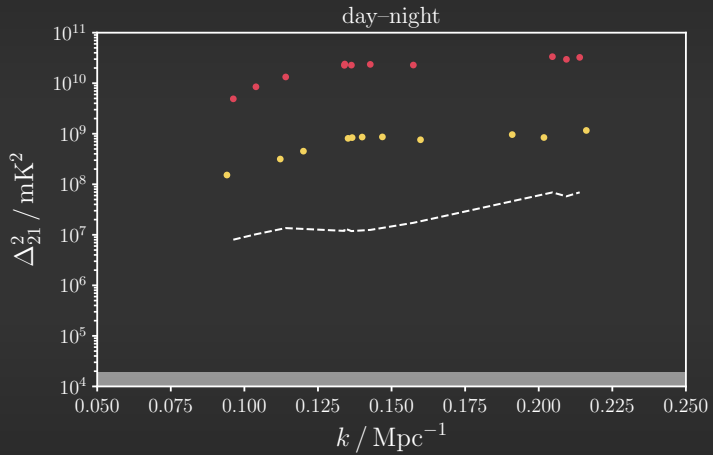


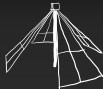
Even–Odd Jackknife





Day–Night Jackknife





Summary

Filtering Illustration

